Journal of The Electrochemical Society, **155** (11) B1145-B1154 (2008)
0013-4651/2008/155(11)/B1145/10/$23.00 © The Electrochemical Society

Characteristic Behavior of Polymer Electrolyte Fuel Cell Resistance during Cold Start

Charles Chacko,[a] Ramaraja Ramasamy,[a,*] Soowhan Kim,[a,b,*] Manish Khandelwal,[a,*] and Matthew Mench[a,,z]**

[a]*Department of Mechanical and Nuclear Engineering, Fuel Cell Dynamics and Diagnostics Laboratory, The Pennsylvania State University, University Park, Pennsylvania 16802, USA*
[b]*Hyundai Motor Corporation, Yongin, Korea*

In this study, experimental constant-current cold starts were performed on a polymer electrolyte fuel cell from −10°C to characterize high-frequency resistance behavior, water motion, and ice accumulation before, during, and after cold start. A diagnostic method for rapid and repeatable cold starts was developed and verified. Cold-start performance is found to be optimized when cell resistance is increasing prior to startup, which is indicative of polymer electrolyte membrane (PEM) dehydration. During cold start, cell resistance initially decreases due to PEM hydration by the product water. Interestingly, after a certain water-uptake capacity of the PEM is reached, resistance increases due to ice formation in and around the cathode catalyst layer (CL), with some evidence of supercooled water flow at low currents. Utilizing lower startup currents apparently does not increase the PEM water-storage capability but does increase the total volume of ice formation in and around the CL. Lower startup currents were found to produce more total heat but at a reduced rate compared to high currents. Therefore, an acceptable current range exists for a given stack design which balances the total heat generation and time required to achieve a successful cold start.
 [DOI: 10.1149/1.2975189]

Manuscript submitted April 28, 2008; revised manuscript received July 30, 2008. Published September 10, 2008.

Polymer electrolyte fuel cells (PEFCs) for automobile applications still have many obstacles to overcome before mass production, including a rapid and damage-free start from frozen conditions. Because water is a product of the fuel cell reaction, operating the PEFC below freezing temperatures is challenging; water produced by the electrochemical reaction can quickly solidify into ice, blocking the reaction sites of the catalyst layer (CL), which can result in a failed start (also known as freeze-out) or accelerate local catalyst and material degradation. Of course, the cell can be heated by external means, but this requires additional energy, ultimately leading to a sacrifice in system efficiency. In an ideal scenario, the heat generated by the electrochemical reaction would raise the cell temperature above 0°C before freeze-out occurs anywhere in the stack, allowing a damage-free self-start.

During cold start, cell performance further suffers due to sluggish kinetics as well as low polymer electrolyte membrane (PEM) conductivity associated with low temperatures.[1-6] Cappadonia et al.[5] showed that conductivity vs temperature (σ vs T) plots of water-saturated Nafion membranes revealed a significant decrease in σ at 0°C, indicating a phase change of water. For fully saturated Gore membranes, Tajiri et al.[4] attributed this decrease in conductivity to residual water diffusing out of the membrane during cool down, freezing, and increasing contact resistance between fuel cell components, which is also consistent with the view of He and Mench.[7-9]

One metric of cold-start performance for a single fuel cell in an isothermal environment is the amount of water produced, m_{pro}, before a freeze-out occurs

$$m_{\text{pro}} = A\frac{M_{\text{H}_2\text{O}}}{2F}\int_{t=0}^{t=\text{freeze-out}} i\,dt \qquad [1]$$

where A is the active area of the fuel cell, $M_{\text{H}_2\text{O}}$ is the molecular weight of water, F is Faraday's constant, t is the time from the beginning of startup until freeze-out, and i is the startup current density. Alternatively, cold-start performance can be described as a success, where the heat generated by the electrochemical reaction raises cell temperature above 0°C (self-start), or as a failure, where the ice formation causes the reaction to cease before the cell rises above 0°C (freeze-out). Many key parameters that affect cold-start performance have been identified in the literature, including membrane water content, startup current density, reactant gas-flow rates, and the phase of product water.

It has been found that a dry membrane state prior to cold start is beneficial, because it increases the membrane water storage capacity.[4,10-14] During cold start, the membrane absorbs some of the product water, prolonging the time until freeze-out occurs. Directly related to membrane water content, the shutdown purge procedure has been shown to play a significant role, as a drier membrane results in increased cold-start performance[12,15] as well as an increased chance of self-start.[16,17] Furthermore, a shutdown purge that removes residual water in the CL has been shown to eliminate freeze/thaw cycle damage.[7-9,18,19] Utilizing a lower startup current density has also been shown to improve cold-start performance in various publications.[4,12,14,20] Specifically, Mao et al.[13] mentioned that lower current densities enable more water to be absorbed into a dry membrane. Tajiri et al.[4] explained that higher current densities may form a ice layer between the CL and diffusion media (DM) and cover reaction sites; hence, the CL pore space is not fully utilized for water storage. During startup, water removal by the reactant gas flow can impact performance as well. Oszcipok et al.[10,11] determined by statistical analysis that cathode air-flow rate significantly affects cold-start performance. It was also demonstrated by Yan et al.[17] that doubling the air-flow rate alone can result in self-start as opposed to freeze-out, indicating that water removal in the vapor phase can play a significant role during cold start. Several in situ imaging studies were performed to determine the phase of product water during cold start. Ishikawa et al.[21,22] showed that liquid water can exist on the cathode CL in a supercooled state at −10°C; however, Ge et al.[15,23] stated that liquid water cannot exist on the cathode CL below −1.5°C.

The behavior of various fuel cell resistances has been studied in literature as well. Oszcipok et al.[10] measured the electrochemical impedance spectra during cold start and determined that high-frequency resistance (HFR) decreases during startup due to membrane hydration by product water. They also showed that charge-transfer resistance increases by an order of magnitude during startup as the electrochemical surface area is reduced by ice coverage. Tajiri et al.[4] also demonstrated that HFR decreases during cold start due to membrane hydration. In a later study, Oszcipok et al.[24] observed that HFR initially decreased, but exhibited a noticeable step increase during startup. This ohmic resistance was divided into membrane resistance and contact resistance; membrane resistance decreased due to membrane hydration, while contact resistance increased due to the freezing of product water. These key cold-start findings from existing literature are summarized in Table I.

* Electrochemical Society Student Member.
** Electrochemical Society Active Member.
z E-mail: mmm124@psu.edu

Table I. Comparison of existing cold-start literature.

Parameter/diagnostic	Key results	Comments
Membrane water content, λ	Dry membrane (low λ) beneficial	Increases membrane water-storage capacity; results in longer cold-start duration until freeze-out[4,9-13]
Shut-down purge technique	Dry shutdown purge beneficial; gives low λ	Produces more water during cold start[4,11,14] Increases chances of self-start[15,16] Reduces freeze/thaw damage[6-8,17,18]
Startup current density, *i*	Low *i* beneficial	Produces more water during cold start[4,11,13,19] Allows more uniform water and ice distribution in cathode CL[4]
Dry air-flow rate	High flow-rate beneficial	Removes more product water before freeze-out[9,10,16]
Phase of product water on cathode CL	Liquid water can exist at −10°C[20,21]	Contradictory with Ref. 14 and 22
	Liquid water cannot exist <−1.5°C[14,22]	Contradictory with Ref. 20 and 21
HFR	HFR decreases during cold start	Due to PEM dehydration[4,9,23]
	HFR increases at the end of cold start[23]	Due to increased contact resistance; not addressed in Ref. 4 and 9

This summary reveals that a gap in fuel cell literature exists regarding the behavior of cell resistance during cold start. This gap gives a motivation to perform experimental cold starts from −10°C to elucidate the behavior of cell resistance before, during, and after cold start. The objective of this study is to develop cell resistance as a diagnostic tool for cold-start performance as well as an indicator for the level of water present in the membrane and CL. Furthermore, the effect of startup current density on cold-start performance, cell resistance, and CL ice formation is investigated. Additionally, it is desired to develop experimental techniques to allow for rapid and repeatable cold starts, because existing approaches require lengthy reconditioning and purge procedures after freeze-out occurs.

Experimental

Experimental setup.— A single 5 cm^2 parallel-channel cell was used in this study. The flow fields consist of 13 straight, parallel channels, each measuring 23 mm long by 1 mm wide and 0.4 mm and 0.6 mm deep on the anode and cathode, respectively. The lands measure 0.75 mm wide, giving a land-to-channel ratio of 0.75. The flow-field plates are 1.3 cm thick gold-plated stainless steel which also serve as current collectors. Outside of the flow-field plates are hollow aluminum end plates to allow coolant fluid to pass through for high-temperature isothermal management. The membrane electrode assemblies (MEAs) used were reinforced Gore Primea 57 series with 0.4 mg/cm^2 Pt loading on each electrode and a dry membrane thickness of 18 μm. Sigracet SGL 10BB, carbon paper with microporous layer and 5% poly(tetrafluorethylene) additive, areal weight of 125 g/m^2, measuring 420 μm ± 70 μm thick, was used as DM for both the anode and cathode. The heat capacity of the fuel cell itself is much greater than that of the MEA; therefore, the heat generated by the electrochemical reaction has a negligible impact on the channel and land boundary temperature during operation. This results in an experimental isothermal boundary condition, although the local membrane and CL temperature can rise during current draw.

A schematic of the experimental configuration is shown in Fig. 1. An Arbin fuel cell test station controlled the electronic load as well as gas-flow rates and dew points. When above freezing, cell temperature was controlled by a Brookfield thermal bath (model EX-200) by passing coolant water at a high flow rate of 2.3 L/min through the coolant channels in the end plates of the cell to assure isothermal operation. A Tenney environmental chamber (model/serial TJR/33631) was used to cool down and sustain cell temperature at −10°C. Cell temperature was measured and recorded in situ using a thermocouple, and it was found that the cell temperature did not vary during the cold start, which can be expected theoretically by a comparison of the relatively small heat produced during startup compared to the large thermal mass of the cold single cell. During cold start, the gas inlet lines to the cell were coiled inside the chamber to allow the reactants to sufficiently cool to the temperature of the chamber before entering the fuel cell. The Arbin humidifiers were bypassed during cold start to ensure dry reactant gas flow. Throughout the experiments HFR measurements were taken to quantify cell resistance using a 5 mA ac current at 3 kHz frequency.

Experimental procedure.— The experimental procedure consisted of four steps: initialization, an extended purge to achieve uniform water distribution within the cell (equilibrium purge), cool down, and consecutive cold starts. After normal preconditioning at 65°C and a baseline performance measurement, the cell was initialized at this same temperature by operation at 600 mV for 30 min under fully saturated conditions, i.e., 100% relative humidity (RH). Hydrogen was supplied to the anode at 0.45 L/min, while air was supplied to the cathode at 1.07 L/min (each flow rate is equivalent to a stoichiometry of 12 at 1.0 A/cm^2). These high flow rates were required to prevent flooding due to the parallel channel design.

The cell was then allowed to cool by natural convection to 37°C for equilibrium purging. The main goal of the equilibrium purge was to achieve a known low membrane water content prior to cool down. A cell temperature of 37°C was chosen to allow the MEA to achieve a dry state during purge, while the humidifiers were held at room temperature. Keeping the humidifiers at room temperature ensured that an insignificant amount of water condensed inside the cell as it

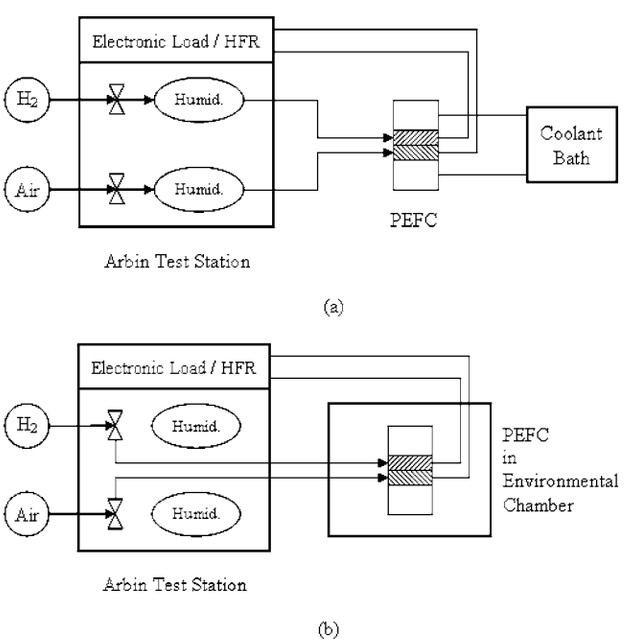

Figure 1. Schematic of test configuration for (a) initialization, performance testing, and equilibrium purge and (b) cool down and cold-start testing.

Table II. Experimental procedure for equilibrium purge cycle (RH = 40%, λ = 3.1).

Step	Stage	Duration (min)	N_2 flow rate (L/min)		Gas dew point (°C)	Cell temperature (°C)
			Anode	Cathode		
I	Purge	180	1.07	1.07	21	37
II	Relaxation	60	0	0	—	37
III	Purge	30	1.07	1.07	21	37
IV	Relaxation	30	0	0	—	37
V	Purge	30	1.07	1.07	21	37
VI	Relaxation	30	0	0	—	Natural cooling

cooled to −10°C. During purging, 40% RH N_2 at 1.07 L/min was fed into the anode and cathode for an extended period of time, which gave a known water activity, a, upon completion. The membrane boundary water activity could then be related to membrane water content, λ, by the Springer relationship[1]

$$\lambda = 0.043 + 17.41a - 39.85a^2 + 36.0a^3 \quad [2]$$

Equation 2 is valid at 30°C for Nafion 117 membranes, although it has been used in many other recent publications over a wide variety of temperatures and for various membrane types. We do have other measurements which show similar behavior for other membranes, although not the type in question. This fact alone does not make the relationship used in Eq. 2 more accurate but rather the only choice currently available in the open literature from which to make a reasonable estimation. Clearly, updated relationships for the particular materials used over a broader range of temperature conditions are needed, although we believe the fundamental nature of the uptake should be similar, so the conclusions drawn based on the use of this relationship will not be significantly altered.

The purge was cycled on and off to determine when equilibrium in all cell components was obtained, because residual water in the DM or CL can rehydrate the membrane. During the off cycle of the purge process, the inlets and outlets of the cell were closed, which allowed the water distribution throughout the MEA and DM to equilibrate to remove any concentration differences that may occur through the MEA|DM structure during purging. The specific details of the purge cycle used to achieve a uniform water distribution of λ = 3.1 for this cell are given in Table II.

After the equilibrium purge, the cell was placed in the environmental chamber and cooled to −10°C. The cell inlets and outlets remained closed in order for λ to stay constant during cool down; the volume of the flow-field channels is 0.3 cm^3, which can condense 4 μg of water during cool down from the dew point of 21°C to −10°C. This amount of water, if fully absorbed by the membrane, gives an increase in λ of only 0.01, which can be neglected. Therefore, λ is assumed to remain constant at 3.1 during the cool-down procedure. The cool-down process took approximately 2.5 h, which included a 1 h soak at −10°C to allow uniform temperature distribution throughout the cell. All cold starts performed in this study occur from −10°C. Prior to cold start, the test station was also purged with dry gas directly from the gas cylinders to remove any residual water that may have accumulated in the pipelines during initialization or purging.

After the cell was sufficiently temperature soaked, dry reactant gases at −10°C were fed into the cell at 0.15 and 0.30 L/min (equivalent stoichiometries of 2.7 and 3.4 at 1.0 A/cm^2) at the anode and cathode, respectively, to allow for open-circuit voltage (OCV) stabilization. Cell resistance was recorded, and once reaching a specific value (0.30 Ω cm^2 unless otherwise specified), the flow rates were changed to 0.05 and 0.11 L/min (equivalent stoichiometries of 12 and 12 at 0.1 A/cm^2) at the anode and cathode, respectively. A cold start was then initiated by drawing a constant current from the cell while cell voltage and resistance were recorded. When cell voltage dropped below a set value (50 mV) due to freeze-out, the electronic load was automatically shut off. In this study, cold-start performance was measured by the amount of water produced during startup, given by Eq. 1. The term "cold-start performance" is defined here as the amount of water produced during the cold-start time until freeze-out occurs. This should not be confused with the generic term of fuel cell performance, which is related to polarization behavior.

It was found that if dry gas continued to flow through the cell after freeze-out (termed cold purge), OCV restabilized due to ice removal by sublimation, and consecutive cold starts could be rapidly performed without the necessity of heating, initializing, and purging the cell again. Cold purging was performed by setting the flow rates back to 0.15 and 0.30 L/min at the anode and cathode, respectively. Once the cell resistance again reached a specific value, the flow rates were changed back to 0.05 and 0.1 L/min on the anode and cathode, respectively, and another cold start could be performed. This cold purge/cold start/cold purge process could then be repeated. The performance of such successive cold starts was quite repeatable and representative of the same behavior seen after a full equilibrium purge. The process is described in more detail in the following sections.

Results and Discussion

Cell resistance during equilibrium purge and cool down.— Cell resistance observed during the equilibrium purge is shown in Fig. 2. As can be seen, resistance increases and plateaus at 0.22 Ω cm^2 during purge periods. During the relaxation periods, resistance decreases due to water redistribution throughout the MEA. The final relaxation period shows a slight increase in resistance because the cell is naturally cooling to room temperature, which decreases membrane conductivity. During purge steps, resistance consistently plateaus around 0.22 Ω cm^2, indicating that at the completion of any purge period the membrane water content is consistently λ = 3.1.

Membrane proton conductivity was measured using HFR by normalizing the cell resistance with respect to the MEA geometry. Con-

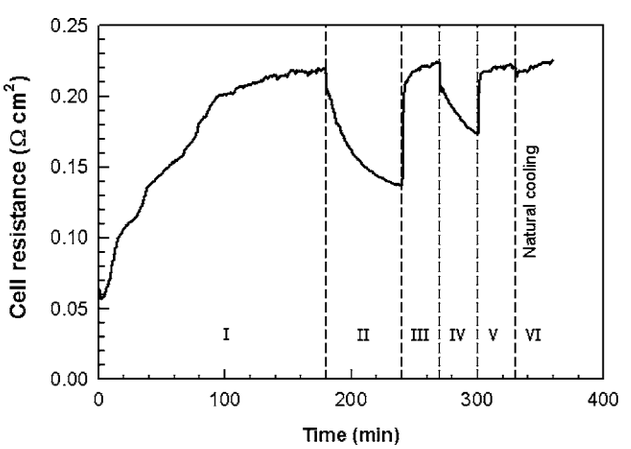

Figure 2. Cell resistance during 40% RH N_2 purge (λ = 3.1). The cell was consecutively purged and relaxed, as labeled.

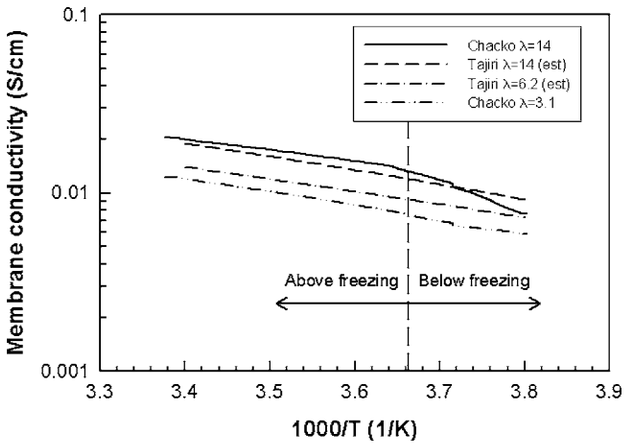

Figure 3. Membrane proton conductivity as a function of temperature and λ during cool down from room temperature to −10°C with comparable data from Tajiri et al.[4]

ductivity measurements could then be determined as the cell cooled from room temperature to −10°C, as shown in Fig. 3. Shown in the Arrhenius form, the σ-*T* relationship for λ = 3.1 shows no noticeable change in slope as the cell cools below freezing, indicating no phase change of water inside the membrane or any appreciable increase in contact resistance. The case of λ = 14 was obtained with a fully humidified membrane and is used as a comparison to the data obtained by Tajiri et al.[4] The σ-*T* curve determined in the present study shows a convex shape. This behavior was also observed by Tajiri et al.,[4] especially at temperatures below −10°C. As described previously, this is believed to be a result of a phase change of water in the membrane and/or an increase in contact resistance due to ice-lens formations between the MEA sublayers. In general, higher conductivities were observed in comparison with data obtained by Tajiri et al.[4] This was also reported by Beuscher et al.,[3] where it was shown that thinner membranes with lower equivalent weights demonstrate higher conductivity values.

Consecutive cold starts.— The behavior of cell resistance during a set of consecutive cold starts can be seen in Fig. 4. Gas flows through the cell during the entire test, but current is only being drawn from the cell during a startup. During startup, cell resistance decreases due to membrane hydration, then increases due to ice formation in the cathode CL. Between cold starts, cell resistance

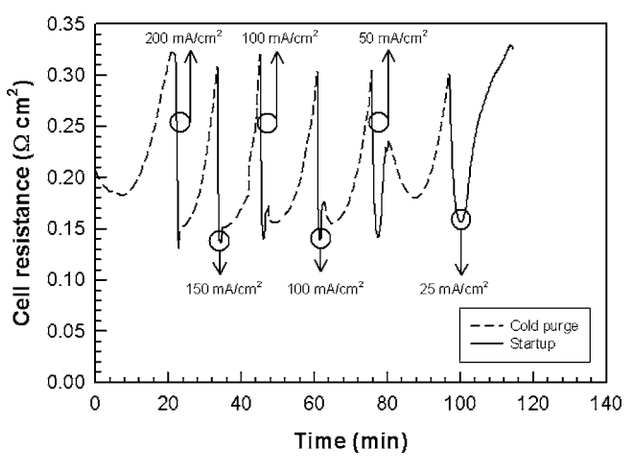

Figure 4. Cell-resistance behavior during a set of consecutive cold starts from various startup current densities.

decreases due to residual ice removal from the cathode CL, then increases due to membrane dehydration. These four processes are described in detail in the following sections. During the entire set of repeated cold starts, the cell temperature was constant and fluctuated no more than 0.2°C. As shown in Fig. 4, the cold starts were initiated once the cell reached a specific resistance value, here 0.30 Ω cm^2, at startup current densities ranging from 200 to 25 mA/cm^2. The case of i = 100 mA/cm^2 was performed twice to ensure the repeatability of tests. Performance proved to be identical; 0.80 mg/cm^2 of water was produced during each startup, and the final resistance recorded at freeze-out was 0.17 Ω cm^2 for each case. A separate study was conducted in order to determine if any difference existed between a startup performed after the long, elevated-temperature equilibrium purge compared to one performed in the middle of a set of rapid, consecutive cold starts. A cold start performed after the equilibrium purge and a cold start performed in the middle of a consecutive set showed less than a 5% difference in voltage and startup time. Furthermore, when the same type of startups shown in Fig. 4 were performed in random order, a negligible difference in voltage and startup time was found. This repeatability indicates that consecutive cold starts can be used as a rapid, efficient, and repeatable cold-start procedure. To compare, the conventional published method requires a four-step process including high-temperature initialization, equilibrium purging, cool down, and cold soak for each cold start performed, which requires approximately 7 h of preparation for only one cold start. Then, after the cold start is initiated and a freeze-out occurs, this 7 h procedure must be repeated. The method of rapid, consecutive cold starts uses the same four aforementioned steps, but the use of the 15 min cold purge after freeze-out allows for an indefinite amount of cold starts to be performed without having to reheat the cell. Thus, this approach significantly reduces experimental time in comparison to conventional published methods[4,10-12,16,17,23,24] and may be used as a rapid and repeatable method to assess cold performance, degradation, and other metrics of interest.

During cold start.— The startups at i = 100 and 50 mA/cm^2 from Fig. 4 are enlarged in Fig. 5a and 5b, respectively. The cell voltage first sharply drops from OCV due to the load applied to the cell. Voltage then slightly increases while resistance decreases due to membrane hydration by the product water. Hydrating the membrane increases proton conductivity, which improves performance (voltage) and decreases resistance and is consistent with previous publications.[4,10,24]

After a certain membrane water-uptake capacity is reached, voltage begins to decrease while cell resistance increases. This behavior is attributed to ice formation in and around the cathode CL. As ice is formed, it begins to cover reaction sites and reduce the electrochemical surface area, and as a result cell voltage decreases. Eventually, the ice completely blocks the CL reaction sites and the electrochemical reaction ceases. Ice should not affect the HFR by merely filling open pores in the CL or DM. This measured resistance increase is therefore indicative of some interfacial ice-lens production or contact loss due to ice expansion. To verify that this resistance increase is indeed a result of ice external to the membrane and not a result of a phase change of water inside the membrane, a cold start was performed but stopped once resistance reached its minimum during startup, which occurs well before freeze-out. The load was removed from the cell and the inlets and outlets were closed, allowing any product water to freeze in the membrane. Resistance was observed to stabilize near the minimum value, indicating that a phase change of the water in the membrane was not responsible for the HFR increase observed during freeze-out. Therefore, it can be concluded that cell resistance does in fact increase due to ice formation during freeze-out.

A simple water balance was performed during cold start, following the modes of transport illustrated in Fig. 6. Initially during startup, the product water is absorbed by the membrane, shown in Fig. 6a. Once the membrane water-uptake capacity is reached, the

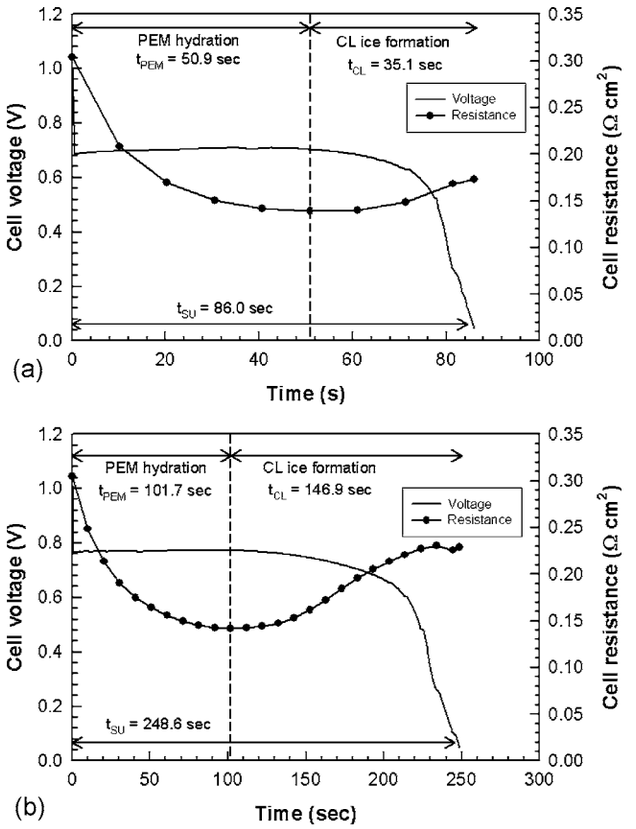

Figure 5. Cell voltage and resistance behavior during cold start for (a) i = 100 and (b) 50 mA/cm^2.

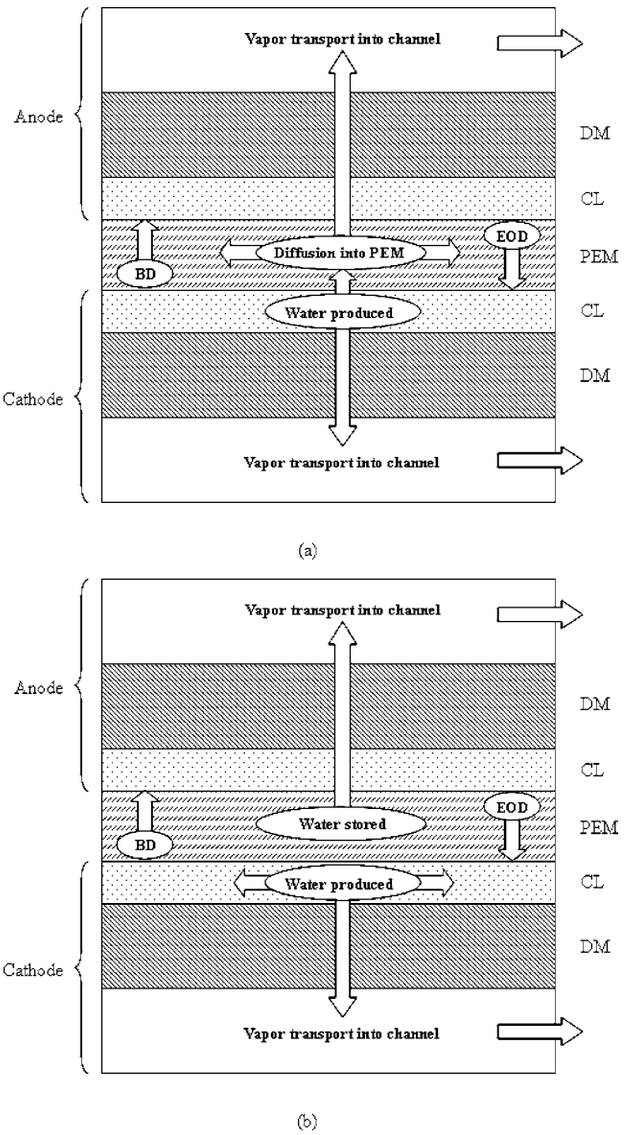

Figure 6. Water transport during cold start: (a) membrane rehydration and (b) catalyst layer ice filling (not to scale).

water begins to fill in and around the cathode CL and freeze, as shown in Fig. 6b. In reality, these two processes might occur in parallel. For analysis purposes, it is assumed that no water freezes in the DM due to low vapor-saturation pressure associated with cold start.[13] Water can be removed from the cell by the anode or cathode gas streams. The effects of electro-osmotic drag (EOD) and back diffusion (BD) are not directly calculated but are incorporated within the calculations of water transport into the membrane or into the cathode CL. For instance, the amount of water that the membrane absorbs, calculated from experimental findings, is affected by the processes of EOD and BD. Therefore, although EOD and BD are not directly calculated, they are incorporated into the water balance.

If the dry reactant gas exits the cell fully saturated, the maximum amount of water removed from the cell is given as[25]

$$m_{\text{rem}} = (\dot{n}_a + \dot{n}_c)\frac{P_{\text{sat}}(T)}{P_{\text{cell}} - P_{\text{sat}}(T)}M_{H_2O}\Delta t \approx (\dot{n}_a + \dot{n}_c)\frac{P_{\text{sat}}(T)}{P_{\text{cell}}}M_{H_2O}\Delta t \quad [3]$$

where $\dot{n}$ is the molar flow rate of the anode or cathode gas stream, $P_{\text{sat}}(T)$ is the saturation pressure of water vapor over either ice or liquid water, P_{cell} is the pressure of the cell, M_{H_2O} is the molecular weight of water, and Δt is the duration of gas flow.

Equation 3 assumes that the gas stream leaving the cell is fully saturated, which may not be the case, depending on the particular cell and operating conditions. In order to approximate the actual saturation level, small desiccant tubes capable of reliably measuring as low as 1 mg of water were attached to the anode and cathode exits of the cell in order to collect the water that is removed by the dry reactant gas streams. This was performed over the course of the set of six consecutive cold starts shown in Fig. 4. It was found that only 17 and 45% of the amount of water calculated by Eq. 3 was actually collected at the anode and cathode, respectively. The low exit saturation level of the anode is expected due to the relatively dry state of the anode during cold start. Based on these calibration tests, the amount of water that is actually removed from the cell during cold-start testing is given as

$$m_{\text{rem}} = (0.17\dot{n}_a + 0.45\dot{n}_c)\frac{P_{\text{sat}}(T)}{P_{\text{cell}}}M_{H_2O}\Delta t \quad [4]$$

Equation 4 is a water-removal calculation assuming constant 17 and 45% saturation levels throughout the entire duration of the set of cold starts. These saturation percentages are dependent on flow rate, water diffusivities through MEA components, and water saturation levels of these components. However, calculations are performed assuming constant saturation percentages of the exit gases throughout the set of cold starts performed in this study.

The water produced during cold start, m_{pro}, is given by Eq. 1, where $t = t_{SU}$ from Fig. 5. The amount of water removed from the cell, m_{rem}, can be determined from Eq. 4, where $\Delta t = t_{SU}$ from Fig. 5. Therefore, the total water stored in the cell, m_{sto}, is given as

Table III. Water balance during cold starts.

		Startup current density, i (mA/cm^2)					
		25	50	100	100	150	200
	Unit	Value					
Overall							
t_{SU}	s	1060.8	248.6	86	85.6	49.2	34.3
m_{pro}	mg/cm^2	2.47	1.16	0.80	0.80	0.69	0.64
m_{rem}	mg/cm^2	0.38	0.09	0.03	0.03	0.02	0.01
m_{sto}	mg/cm^2	2.09	1.07	0.77	0.77	0.67	0.63
PEM hydration							
t_{PEM}	s	183.1	101.7	50.9	51.9	30.5	27.3
$m_{PEM,act}$	mg/cm^2	0.36	0.44	0.46	0.47	0.42	0.50
$m_{PEM,max}$	mg/cm^2	0.95	0.95	0.95	0.95	0.95	0.95
$(act/calc)_{PEM}$	mg/cm^2	38	46	48	49	44	52
CL ice formation							
t_{CL}	s	877.7	146.9	35.1	33.7	18.7	7.0
$m_{CL,act}$	mg/cm^2	1.73	0.63	0.31	0.30	0.25	0.13
$m_{CL,max}$	mg/cm^2	0.65	0.65	0.65	0.65	0.65	0.65
$(act/calc)_{CL}$	mg/cm^2	268	98	49	47	39	20

$$m_{sto} = m_{pro} - m_{rem} \quad [5]$$

The water stored in the cell is utilized for either membrane hydration or cathode CL ice formation. During cold start, the membrane stores an amount of water, $m_{PEM,act}$, given by

$$m_{PEM,act} = m_{sto}\frac{t_{PEM}}{t_{SU}} \quad [6]$$

where t_{PEM} and t_{SU} are determined from Fig. 5. The maximum amount of water that the membrane can store, $m_{PEM,max}$, is given as

$$m_{PEM,max} = M_{H_2O}\delta_{PEM}\frac{\rho_{dry}(\lambda_{sat} - \lambda_i)}{EW}A \quad [7]$$

Typical membrane properties are assumed: $\delta_{PEM} = 18$ μm, $\rho_{dry} = 2000$ kg/m^3, $EW = 0.95$ kg/mol, and $\lambda_{sat} = 14$. Because the membrane is dried to some degree prior to startup, the exact value of λ_i, the initial membrane water content prior to startup, is difficult to determine (see Between Cold Start section), but it is assumed that the membrane is dried to $\lambda_i < 3.1$ prior to startup. For water-storage calculation purposes only, we consider the membrane to be completely dry at startup, i.e., $\lambda_i = 0.043$. This assumption accounts for the absolute maximum amount of water the membrane can uptake (although it is not realistic to fully dry the membrane).

The amount of water that is utilized for cathode CL ice formation, $m_{CL,act}$, is given as

$$m_{CL,act} = m_{sto}\frac{t_{CL}}{t_{SU}} \quad [8]$$

where t_{CL} and t_{SU} are determined from Fig. 5. The maximum amount of ice that the cathode CL can store, $m_{CL,max}$, is given as

$$m_{CL,max} = \delta_{CL}\left(\varepsilon_{CL}\rho_{ice} + \lambda_{sat}\varepsilon_{CL,e}\frac{\rho_{dry}}{EW}M_{H_2O}\right)A \quad [9]$$

The left term in parentheses in Eq. 9 represents the amount of water that can be stored in the pores of the cathode CL, while the right term represents the amount of water that can be stored in the electrolyte phase of the cathode CL. Typical CL properties are assumed: $\delta_{CL} = 10$ μm, $\varepsilon_{CL} = 0.6$, and $\varepsilon_{CL,e} = 0.2$. To account for the maximum cathode CL ice-storage capacity, it is assumed the CL is completely free of ice prior to startup and becomes fully saturated at freeze-out, i.e., $\lambda_{sat} = 14$.

The calculated quantities of the water balance for the cold starts shown in Fig. 4 are given in Table III. The actual amount of water stored in the membrane is relatively constant for all cases, indicating that using a lower startup current density does not allow for more utilization of the membrane storage capacity during the start-up time. Even if it is assumed that water diffusion out of the membrane is extremely low and the membrane dehydration region prior to startup keeps the membrane at $\lambda_i = 3.1$ (and not completely dry as assumed for maximum storage calculations), the membrane storage utilization only increases to 62% for the $i = 100$ mA/cm^2 case, again indicating the membrane is not fully saturated at freeze-out.

In order to analyze this membrane water-storage phenomenon, the time constant for diffusion through the membrane can be found using

$$\tau_{diff} = \frac{\delta_{PEM}^2}{D} \quad [10]$$

Taking the minimum diffusion constant of water into the membrane over various λ ($D = 6 \times 10^{-12}$ m^2/s),[26] this time constant is calculated to be 54 s. Based on the time associated with membrane hydration for $i = 25$ mA/cm^2 ($t_{PEM} = 183$ s), the product water should have ample time to fully diffuse into the membrane. However, much less than the maximum membrane storage capacity is utilized under these conditions. It is concluded that for a relatively dry membrane, under the conditions tested, the water uptake into the membrane was limiting, and therefore ice formed in the catalyst layer and the cell suffered from freeze-out before complete uptake could be achieved. The average membrane water storage of 0.44 mg/cm^2 gives a $(\Delta\lambda)_{max} = 6.4$ according to Eq. 7. Therefore, in order to optimize cold-start performance by keeping the membrane as hydrated and conductive as possible but also allowing it to store 0.44 mg/cm^2 of water, there is an optimal membrane water content prior to startup. This depends on the maximum water content of the membrane, λ_{max}, before ice begins to form. For instance, if $\lambda_{max} = 14$ in a frozen state, the optimal membrane water content prior to startup would be $\lambda_i = 7.6$. That is, as λ increases from 7.6 to 14 during cold start, the membrane can store 0.44 mg/cm^2 of product water while also staying as conductive as possible. An initial condition of $\lambda_i < 7.6$ would not serve any purpose, as the additional capacity could not be utilized before ice begins to form.

The amount of water that freezes in the cathode CL increases as startup current density decreases. This implies that a lower current density allows for water to distribute itself more within the CL prior to freeze-out, which is consistent with existing literature.[4] However, for $i = 25$ mA/cm^2, the actual ice produced is over two times greater than the cathode CL storage capacity. This indicates that some of the water stored during cold start emerges out of the cathode CL and is stored in the DM, also reported by Mao et al.[14] The fact that this water has the ability to be transported out of the CL (as solid ice

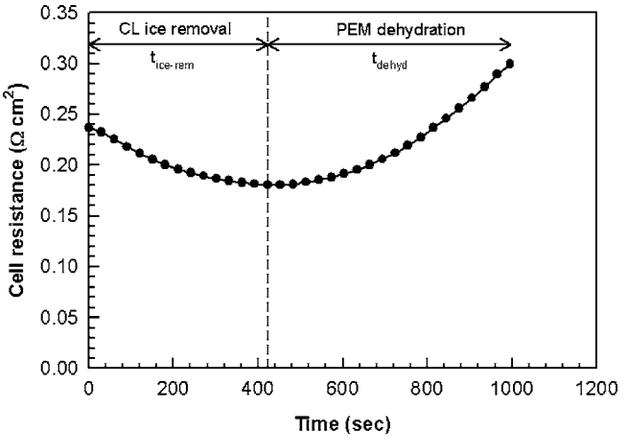

Figure 7. Cell-resistance behavior between cold start, after $i = 50$ mA/cm^2 and prior to $i = 25$ mA/cm^2 startup. Gas flows through the cell while OCV stabilizes.

would not have this transport ability) may be indicative of the presence of supercooled liquid water, as observed by Ishikawa et al.[21,22] at −10°C. This water then freezes inside the DM or gas channels. The effect of ice production on cell resistance is examined later in this study.

Between cold starts.— Resistance behavior between cold starts (during the cold purge) is a direct consequence of the dry gas removing residual product water/ice from the cell. Figure 7 shows cell resistance behavior between the cold start of $i = 50$ and 25 mA/cm^2 (note that no current is being drawn from the cell). Resistance is seen to initially decrease due to residual ice removal from the CL. Once this ice is removed from the CL, resistance then increases due to membrane dehydration. Again, these processes may occur in parallel as well.

A simple water balance was performed on the data of Fig. 7. While the cathode gas stream first removes ice from the cathode CL and then begins to dehydrate the membrane, the anode gas stream is believed to only dehydrate the membrane, because there is little water to remove from the anode CL. The amount of ice removed from the cathode CL can be found using Eq. 4 and accounting for only the cathode gas stream, where $\Delta t = t_{ice\text{-}rem} = 422$ s. The amount of water removed from the membrane can be found using Eq. 4 as well and accounting for each gas stream separately; $\Delta t = t_{dehyd,a} = 996$ s and $\Delta t = t_{dehyd,c} = 574$ s for the anode and cathode, respectively. The amount of ice or water that was stored in the CL or membrane is given in Table III as $m_{CL,act}$ and $m_{PEM,act}$, respectively. Based on this water balance, it is found that the removal calculation underestimates the CL ice storage by 42% and overestimates the membrane water storage by 66%. The reason for this discrepancy is believed to be a result of the parallel processes of membrane hydration, and CL ice formation during startup as well as CL ice removal and membrane dehydration during cold purge. Furthermore, the specific saturation levels of the exit gases likely depend on the saturation level of water and the diffusivities of water out of each specific component. Because of this discrepancy, an overall water-balance analysis was performed during and after the cold starts shown in Fig. 4 to validate Eq. 4. In order for the water balance to equate, the amount of water stored in the cell during a cold start, m_{sto}, must be equal to the water removed during cold purge after that particular cold start, m_{rem}. These values are shown in Table IV and it is found that the total water removed overestimates the total water stored by only 0.06 mg/cm^2 during the entire set. This validates the conclusion that Eq. 4 correctly calculates the overall amount of water removed from the cell but should not be used to specifically account for the amount of ice removed from the CL vs the amount of water removed from the membrane.

Table IV. Overall water balance during set of consecutive cold starts.

		Startup current density, i (mA/cm^2)					
		200	150	100	100	50	Total
	Unit	Value					
m_{sto}	mg/cm^2	0.63	0.67	0.77	0.77	1.07	3.91
m_{rem} [a]	mg/cm^2	0.66	0.63	0.81	0.78	1.09	3.97
m_{sto}-m_{rem}	mg/cm^2	−0.03	0.04	−0.04	−0.01	−0.02	−0.06

[a] These values were calculated after the above-listed cold start.

Effect of startup current density.— Figure 8 plots cold-start performance, measured in amount of water produced, as a function of startup current density. The reactant gas-flow rates, given in the Experimental section, remained consistent during these cold starts. Therefore, the water stored in the cell is a more suitable performance measurement between the different startup current-density cases. The final cell resistance, recorded at freeze-out, is also shown. Figure 8 shows that a lower startup current density does in fact give better cold-start performance, because a lower current density allows water to distribute more evenly in the CL before freeze-out.[4] This additional water in and around the CL leads to additional ice, which is indicated by a higher final resistance.

Figure 9 demonstrates how the amount of ice stored during startup (reference $m_{CL,act}$ in Table III) affects final cell resistance. The upper axis shows the ratio of ice stored during each cold start to the maximum storage capacity of the cathode CL. As more ice is stored during the CL ice-formation stage of startup, ice fills in and around the cathode CL. Consequently, the final cell resistance recorded at freeze-out increases. This trend demonstrates that cell resistance at freeze-out is an indicator of ice content in and around the CL.

To further investigate the effect of water production on cell-resistance values, the minimum resistance recorded during startup is plotted in Fig. 10 as a function of the water produced during startup that is utilized for membrane hydration (reference $m_{PEM,act}$ in Table III). In general, if more water hydrates the membrane, the cell resistance is lower, which is expected, and as the membrane hydrates, proton conductivity increases. However, this is not a particularly strong relationship. The maximum difference in resistance for this cell and these materials is only 18 mΩ cm^2. The upper axis in Fig. 10 plots the ratio of water utilized for membrane hydration to the maximum water storage capacity of the membrane, which is a weak function of startup current density. This further reinforces the point that the membrane can only absorb a certain amount of water during startup regardless of startup current density.

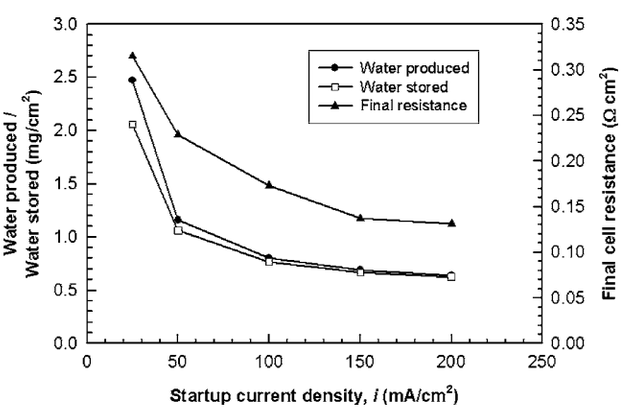

Figure 8. Water produced, water stored, and final resistance during cold start as a function of startup current density.

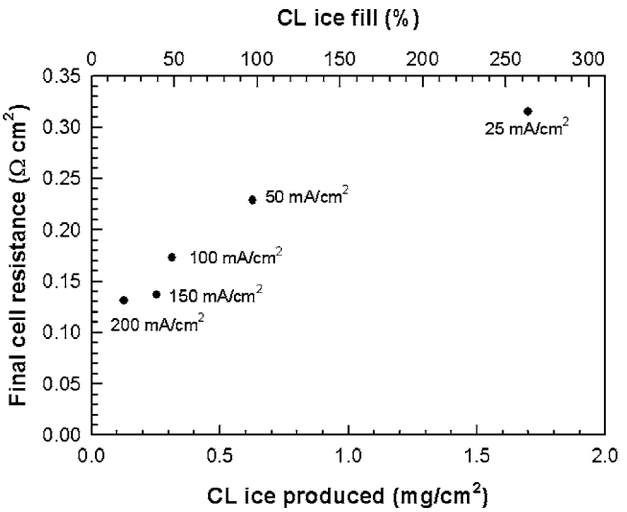

Figure 9. Cell resistance recorded at freeze-out as a function of ice produced in the CL. Upper axis shows percentage of CL ice-storage capacity utilized.

Other useful performance measurements that can be extracted from these startups include the total energy produced (E) and total heat generated (Q) by the cell during cold start, given below

$$E = \int_{t=0}^{t_{SU}} V_{cell} i A dt \quad [11]$$

$$Q = \int_{t=0}^{t_{SU}} (E_{th} - V_{cell}) i A dt \quad [12]$$

where V_{cell} is the actual cell voltage and E_{th} is the thermal potential (E_{th} = 1.48 V). Furthermore, the average energy-generation rate ($\dot{E}_{avg}$) and average heat-generation rate ($\dot{Q}_{avg}$) during cold start can be calculated by

$$\dot{E}_{avg} = V_{cell,avg} i A \quad [13]$$

$$\dot{Q}_{avg} = (E_{th} - V_{cell,avg}) i A \quad [14]$$

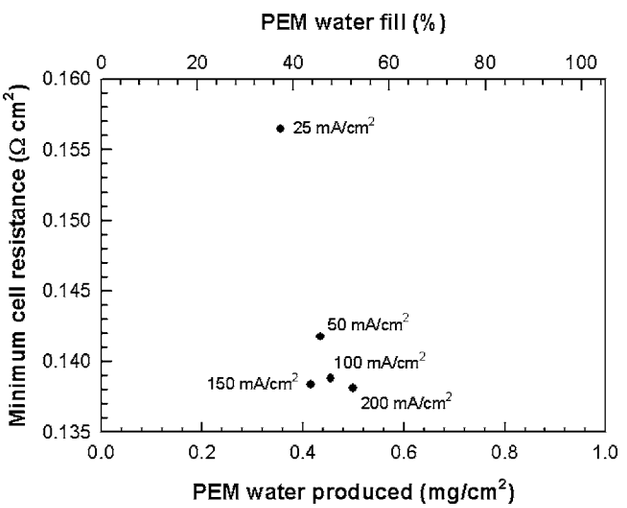

Figure 10. Minimum resistance recorded during startup as a function of the water used for membrane hydration. Upper axis shows percentage of maximum membrane water-storage capacity utilized.

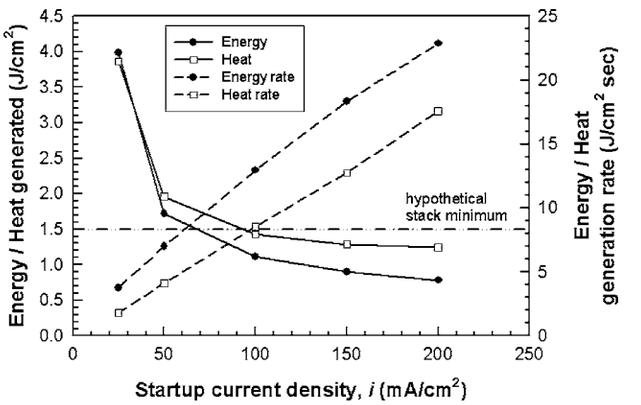

Figure 11. Total energy produced, total heat produced, average energy production rate, and average heat production rate during cold start as a function of startup current density.

These calculated quantities can be seen as a function of startup current density in Fig. 11. Both total energy produced and total heat produced follow a power-law relationship, indicating that a lower startup current density is able to produce more usable energy as well as generate more heat to aid in self-start. This is attributed to lower startup current densities giving longer operation times before freeze-out; the total energy/heat produced is more dependent on startup time than current density in the range of parameters tested. However, when comparing the average production rates of energy and heat, it can be seen that these rates increase linearly as a function of startup current density. Therefore, a compromise must be made between total energy/heat produced and their subsequent rates. This compromise can be used to provide an operational guideline for rapid stack startup. For instance, a certain fuel cell stack may have a minimum total heat required to self-start (indicated by the "hypothetical stack minimum" line in Fig. 11). In order to generate sufficient heat for self-start and do so as rapidly as possible, a startup current density of approximately i = 90 mA/cm^2 would be optimal.

Predicting cold-start performance with initial resistance.— The results discussed so far conclude that the general hydration state of the MEA and the presence of residual ice can be described by measured HFR. Because cold-start performance is highly dependent on MEA water content, the cell resistance recorded prior to startup may be used to predict performance. HFR is well suited for this diagnostic due to its fast and nonintrusive nature. An additional set of experiments were performed to determine the range of resistance values that lead to optimal cold-start performance. For these experiments, startup current density, flow rate, and cell temperature were identical for all cases; the only difference was initial cell resistance. Figure 12 shows cold-start performance as a function of initial resistance for 50 different cold starts. There are four different "zones" of resistance values, which can be related to Fig. 7, that give significantly different cold-start performance. The first zone, "Residual ice in CL," corresponds to "CL ice removal" in Fig. 7, indicative of residual ice being present in the CL from the previous startup. This gives quite a poor performance, because the reaction sites of the CL are still partially covered or filled with ice. The second zone, "Transition between ice in CL and dry PEM," corresponds to the minimum value of resistance shown in Fig. 7 and is representative of the transition between CL ice removal and membrane dehydration. This zone gives a large amount of scatter in performance, because this transition is nondistinct; the processes of CL ice removal and membrane dehydration are in parallel. The "Dry PEM" corresponds to the "PEM dehydration" region seen in Fig. 7 and gives optimal and most predictable performance. This further reinforces the point that a dry membrane is beneficial for cold start. However, there is a region, "PEM too dry," where the membrane is

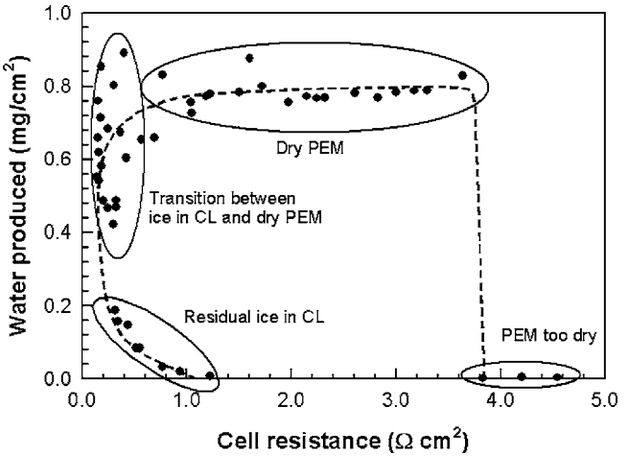

Figure 12. Cold-start performance as a function of cell resistance immediately prior to cold start, startup current density, $i = 100$ mA/cm^2. Each data point signifies a single cold start.

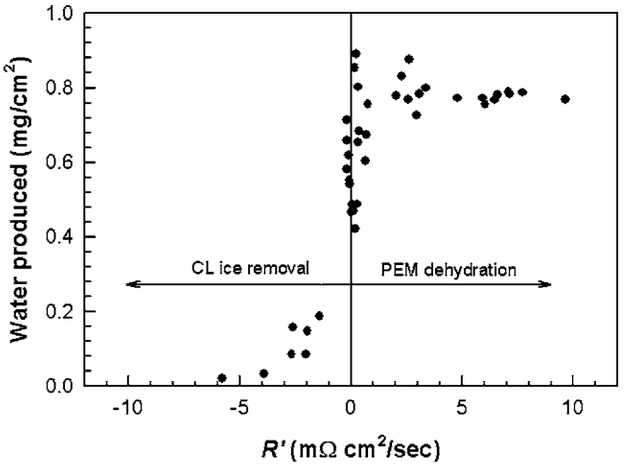

Figure 13. Cold-start performance as a function of R', startup current density, $i = 100$ mA/cm^2. Each data point signifies a single cold start.

too dry and therefore has a high resistivity, which does not allow current to be drawn from the cell. The cut-off for this region is approximately 3.83 Ω cm^2 for this cell. In order to ensure a dry PEM and therefore optimal cold-start performance for the cell tested, HFR prior to startup should range between 1.3 and 3.7 Ω cm^2.

The duality of values seen in Fig. 12 is due to the path-dependent nature of cell resistance. Once again referencing Fig. 7, a high resistance may be caused by CL ice or a dehydrated membrane. Understanding the cause of a specific cell resistance value is of vast importance and can be determined by the rate of change in resistance, denoted R'. Here the parameter R' is introduced, which utilizes the last two resistance measurements prior to startup and quantifies the resistance change over time immediately prior to a cold start

$$R' = \frac{dR}{dt} = \frac{\Delta R}{\Delta t} = \frac{R_2 - R_1}{t_2 - t_1} \quad [15]$$

A decrease in cell resistance, signified by a negative value of R', represents ice removal from the CL. An increase in cell resistance, signified by a positive value of R', represents membrane dehydration. A zero value of R' is representative of minimum resistance achievable, which is the transition between CL ice removal and membrane dehydration. Figure 13 is a plot of the performance values associated with Fig. 12 as a function of R'. The values in the region of "PEM too dry" are left out for clarity. As can be seen, a negative value of R' gives poor performance due to residual ice remaining in the CL. A zero value of R' gives a large amount of scatter, due to the nondistinct transition between CL ice removal and membrane dehydration. A positive value of R' gives optimal and repeatable cold-start performance, which is a metric that can be used to ensure a positive startup in stacks.

Conclusions

Cold starts were performed from −10°C in order to understand and diagnose the behavior of cell voltage and resistance. A method of performing rapid and repeatable cold starts was introduced. This method allows for successive cold starts to be performed without the necessity of reheating the cell, significantly reducing the time required for experimental cold starts. This method may also be employed to conduct extended cold-start durability testing on a much quicker time scale than previous methods.

HFR has proven to be a key electrochemical diagnostic tool for cold-start behavior and performance. Prior to cold-start, cell resistance initially decreases due to CL ice removal, then increases due to membrane dehydration. The parameter R' was introduced which measures the rate of change in cell resistance prior to startup. Optimal cold-start performance occurs when R' is positive, indicating membrane dehydration. Negative values of R', indicative of residual ice remaining in the CL, give a poor cold-start performance.

During cold start, cell resistance initially decreases due to membrane hydration, then increases due to CL ice formation. It was found that for the conditions tested, the water uptake into a dry membrane was slower than the ice formation, and freeze-out occurred before full membrane rehydration. Based on this water-absorption capability, the maximum change in average membrane water content was determined to be $(\Delta\lambda)_{max} \cong 6.4$. It was also found that lower startup current densities give a higher cell resistance at freeze-out. This higher final resistance is indicative of more ice being present in and around the CL at freeze-out. During freeze-out, lower startup current densities can produce more water than the cathode CL can theoretically store. This may be a sign of supercooled liquid water diffusing out of the CL and freezing in the DM and CL|DM interface.

Using a lower startup current density gives better cold-start performance in terms of total water, energy, and heat produced. However, lower startup current densities have slower production rates of each of these quantities. Regarding rapid stack startup, an optimal startup current density exits such that sufficient heat is generated to raise the stack above 0°C as quickly as possible.

Acknowledgments

The authors are grateful to NSF CAREER award no. 0644811 and The Pennsylvania State University Mechanical and Nuclear Engineering Department for support as well as W. L. Gore and Associates for supplying MEA samples.

The Pennsylvania State University assisted in meeting the publication costs of this article.

List of Symbols

A	cross-sectional area, m^2
a	water activity
D	diffusion of water into membrane, m^2/s
E	energy, J
E_{th}	thermal potential, V
$\dot{E}$	energy-generation rate, J/s
EW	equivalent weight, kg/mol
F	Faraday's constant, 96,487 C/mol eq
i	current density, A/m^2
m	mass of water, kg
M_{H_2O}	molecular weight of water, 0.018 kg/mol
$\dot{n}$	molar flow rate, mol/s
P	pressure, atm
Q	heat, J
$\dot{Q}$	heat generation rate, J/s
R'	resistance change over time, $\Omega\ m^2/s$
t	time, s
T	temperature, K

Greek

Δ	change
δ	thickness, m
ε	porosity
$\varepsilon_{CL,e}$	volume fraction of ionomer in CL
λ	membrane water content, # H_2O/SO_3^-
ρ	density, kg/m^3
σ	membrane conductivity, S/m
τ	diffusion time coefficient, s

Subscript

a	anode
act	actual
avg	average
c	cathode
cell	cell
CL	catalyst layer
dehyd	dehydration
diff	diffusion
dry	dry
i	initial
PEM	polymer electrolyte membrane
pro	produced
rem	removed
sat	saturation
sto	stored
SU	startup

References

1. T. E. Springer, T. A. Zawodzinski, and S. Gottesfeld, *J. Electrochem. Soc.*, **138**, 2334 (1991).
2. T. A. Zawodzinski, T. E. Springer, J. Davey, J. Valerio, and S. Gottesfeld, in *Modeling of Batteries and Fuel Cells*, R. E. White, M. W. Verbrugge and J. F. Stockel, Editors, PV 91-10, p. 187, The Electrochemical Society Proceedings Series, Pennington, NJ (1991).
3. U. Beuscher, S. J. C. Cleghorn, and W. B. Johnson, *Int. J. Energy Res.*, **29**, 1103 (2005).
4. K. Tajiri, Y. Tabuchi, and C. Y. Wang, *J. Electrochem. Soc.*, **154**, B147 (2007).
5. M. Cappadonia, J. W. Erning, S. M. Saberi Niaki, and U. Stimming, *Solid State Ionics*, **77**, 65 (1995).
6. E. L. Thompson, J. Jorne, W. Gu, and H. A. Gasteiger, *J. Electrochem. Soc.*, **155**, B625 (2008).
7. S. He and M. M. Mench, *J. Electrochem. Soc.*, **153**, A1724 (2006).
8. S. He, S. H. Kim, and M. M. Mench, *J. Electrochem. Soc.*, **154**, B1024 (2007).
9. S. He, J. H. Lee, and M. M. Mench, *J. Electrochem. Soc.*, **154**, B1227 (2007).
10. M. Oszcipok, D. Riemann, U. Kronenwett, M. Kreideweis, and M. Zedda, *J. Power Sources*, **145**, 407 (2005).
11. M. Oszcipok, M. Zedda, D. Riemann, and D. Geckeler, *J. Power Sources*, **154**, 404 (2006).
12. K. Tajiri, Y. Tabuchi, F. Kagami, S. Takahashi, K. Yoshizawa, and C. Y. Wang, *J. Power Sources*, **165**, 279 (2007).
13. L. Mao and C. Y. Wang, *J. Electrochem. Soc.*, **154**, B139 (2007).
14. L. Mao, C. Y. Wang, and Y. Tabuchi, *J. Electrochem. Soc.*, **154**, B341 (2007).
15. S. Ge and C. Y. Wang, *Electrochim. Acta*, **52**, 4825 (2007).
16. M. Khandelwal, S. Lee, and M. M. Mench, *J. Power Sources*, **172**, 816 (2007).
17. Q. Yan, H. Toghiani, Y. W. Lee, K. Liang, and H. Causey, *J. Power Sources*, **160**, 1242 (2006).
18. S. Kim and M. M. Mench, *J. Power Sources*, **174**, 206 (2007).
19. S. Kim, B. K. Ahn, and M. M. Mench, *J. Power Sources*, **179**, 140 (2008).
20. Y. Hishinuma, T. Chikashisa, F. Kagami, and T. Ogawa, *JSME Int. J., Ser. B*, **47**, 234 (2004).
21. Y. Ishikawa, T. Morita, K. Nakata, K. Yoshida, and M. Shiozawa, *ECS Trans.*, **1**(6), 359 (2006).
22. Y. Ishikawa, T. Morita, K. Nakata, K. Yoshida, and M. Shiozawa, *J. Power Sources*, **163**, 708 (2007).
23. S. Ge and C. Y. Wang, *Electrochem. Solid-State Lett.*, **9**, A499 (2006).
24. M. Oszcipok, A. Hakenjos, D. Riemann, and C. Hebling, *Fuel Cells*, **2**, 135 (2007).
25. M. M. Mench, *Fuel Cell Engines*, John Wiley & Sons, Inc., New York (2008).
26. F. Jiang, W. Fang, and C. Y. Wang, *Electrochim. Acta*, **53**, 610 (2007).